Depth porosity relationships and virgin specific storage estimates for the Upper Sante Fe Group aquifer system, central Albuquerque Basin, New Mexico

William C. Haneberg

New Mexico Geology, v. 17, n. 4 pp. 62-71, Print ISSN: 0196-948X, Online ISSN: 2837-6420.
https://doi.org/10.58799/NMG-v17n4.62

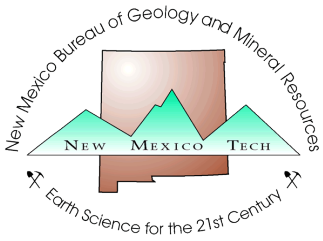

This page is intentionally left blank to maintain order of facing pages.

Depth-porosity relationships and virgin specific storage estimates for the upper Santa Fe Group aquifer system, central Albuquerque Basin, New Mexico

by *William C. Haneberg*, New Mexico Bureau of Mines and Mineral Resources, 2808 Central SE, Albuquerque, NM 87106

Abstract

Model depth-porosity curves fitted to geophysical log porosity data for five water wells in the Albuquerque area show that depth-porosity relationships in upper Santa Fe Group sediments follow trends similar to those in other basins. Goodness-of-fit values were higher for logarithmic type curves than for exponential type curves and suggest that compaction may account for 10% to 50% of the observed porosity variability. The remainder is attributed to stratigraphic variability. Depth-averaged virgin specific storage values range from approximately 2×10^{-4} to 5×10^{-4} m^{-1}. Specific compaction estimates, calculated by assuming that the effective aquifer thickness is nearly the same as a typical City of Albuquerque well screen length of approximately 200 m, ranged from 0.02 to 0.10 m/m. The absence of widespread subsidence in the basin suggests that Santa Fe Group sediments in the Albuquerque Basin are overconsolidated; thus, land subsidence caused by the dewatering of upper Santa Fe Group aquifers should not become a significant problem until the preconsolidation stress is exceeded. Geomorphic evidence suggests that the overconsolidation is a consequence of the Pleistocene incision of the Rio Grande valley, which produced about 100 m of topographic relief and an estimated preconsolidation stress on the order of 1,000 ±200 kPa (100 ±20 m H_2O) greater than the current lithostatic effective stress.

Introduction

Geophysical logs from Albuquerque Basin water wells, as well as those from other sedimentary basins throughout the world, typically show a systematic decrease in porosity with depth that is generally believed to result from the compaction of sediments as they are buried and subjected to increasing lithostatic stresses. Athy (1930), Dickinson (1953), Baldwin and Butler (1985), Helm (1984) and others have quantified these depth-porosity relationships using logarithmic or exponential depth-porosity curves for various basins, and Helm (1984) summarizes past attempts to use depth-porosity curves as a basis for the calculation of virgin specific storage estimates.

More than half of the sediment compaction predicted by generic depth-porosity curves occurs within 100 m of the surface, and about two-thirds of the sediment compaction occurs within 500 m of the surface (Haneberg, 1988). The shallow depths of basin-fill aquifer systems—such as the upper Santa Fe Group in the Albuquerque area—therefore make them especially susceptible to compaction. There may be, for example, significant changes in porosity and storage between the top and the bottom of a thick aquifer. For the same reason, porosity measurements obtained from outcrop samples at the surface may seriously overestimate porosity values at depth. Accurate assessment of the volume of ground water available in a basin, therefore, requires some knowledge of depth-porosity relationships, which can be provided by depth-porosity curves. Depth-porosity curves are also important because they are, in essence, stress-strain curves that allow the hydrogeologist to predict the effects of ground-water overdraft by examining the effects of increasing effective stress on sediment compaction and, consequently, land subsidence at the Earth's surface (Helm, 1984). This is possible because the increase in lithostatic stress with depth is mechanically equivalent to the increase in effective stress caused by a decrease in hydraulic head (or, more specifically, pore-water pressure). Predictions of aquifer system compaction potential are important because they provide some basis for including the economic costs of subsidence-induced infrastructure damage in ground-water development strategies.

Purpose and scope

The work described in this paper was undertaken in order to obtain first-order estimates of (1) the importance of sediment compaction in controlling porosity variability within basin-fill aquifer units and (2) the compaction potential of the basin-fill aquifer system. To accomplish this, porosity logs were analyzed for the five Albuquerque Basin water wells (Charles 5, Coronado 2, Gonzales 1, PSMW 19, and Zamora 1 wells; Fig. 1). These wells were selected because digital data files were either on-hand at or could be obtained easily by the New Mexico Bureau of Mines and Mineral Resources. Although digital log files are available for other city wells, the expense of obtaining the files for more than a handful of wells was prohibitive. Scales of porosity variability were first examined by constructing porosity variograms on a lithofacies-by-lithofacies basis for the Charles 5 well. Exponential and logarithmic type porosity curves were then fitted to geophysical log density porosity data sets for all five wells, and depth-averaged virgin specific storage and specific compaction estimates were calculated using methods developed by Helm (1984). Finally, the potential for land subsidence as a consequence of upper Santa Fe Group compaction is discussed in light of both the quantitative estimates made in this paper and the Cenozoic geomorphic history of the Albuquerque area.

Hydrogeologic setting

The geologic evolution and hydrogeologic setting of the Albuquerque Basin are discussed in detail by Hawley (in press a,b). The five wells analyzed in this paper are fortuitously distributed throughout

New Mexico GEOLOGY

• Science and Service

ISSN 0196-948X

Volume 17, No. 4, November 1995

Editor: Carol A. Hjellming

EDITORIAL BOARD
Steve M. Cather, *NMBMMR*, Chairman
Thomas Giordano, *NMSU*
Laurel B. Goodwin, *NMIMT*
Spencer G. Lucas, *NMMNHS*
Frank J. Pazzaglia, *UNM*

Published quarterly by
New Mexico Bureau of Mines and Mineral Resources
a division of New Mexico Institute of Mining and Technology

BOARD OF REGENTS
Ex-Officio
Gary Johnson, *Governor of New Mexico*
Alan Morgan, *Superintendent of Public Instruction*
Appointed
J. Michael Kelly, *Pres.*, 1992–1997, *Roswell*
Steve S. Torres, *Sec./Treas.*, 1991–1997, *Albuquerque*
Diane D. Denish, 1992–1997, *Albuquerque*
Delilah A. Vega, *Student Member*, 1995–1997, *Socorro*
Charles A. Zimmerly, 1991–1997, *Socorro*

New Mexico Institute of Mining and Technology
President . . . . . Daniel H. López

New Mexico Bureau of Mines and Mineral Resources
Director and State Geologist . . . . . Charles E. Chapin

Subscriptions: Issued quarterly, February, May, August, November; subscription price $6.00/calendar year.

Editorial Matter: Articles submitted for publication should be in the editor's hands a minimum of five (5) months before date of publication (February, May, August, or November) and should be no longer than 20 typewritten, double-spaced pages. All scientific papers will be reviewed by at least two people in the appropriate field of study. Address inquiries to Carol A. Hjellming, Editor of *New Mexico Geology*, New Mexico Bureau of Mines and Mineral Resources, Socorro, New Mexico 87801-4796.

Circulation: 1,400

Printer: University of New Mexico Printing Services

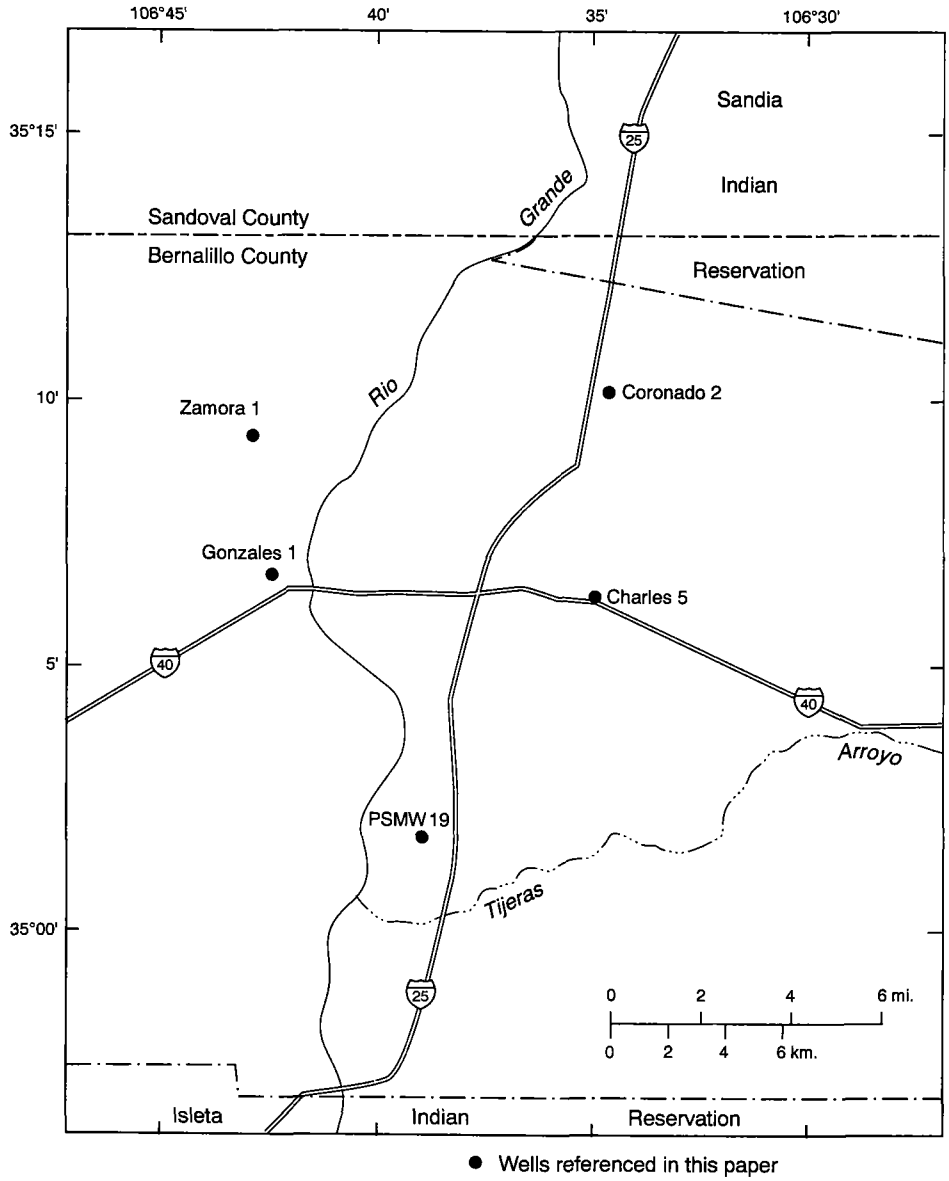

FIGURE 1—Index map of the Albuquerque area showing locations of wells referenced in this paper.

the Albuquerque metropolitan area and, more importantly, were drilled in areas where Thorn et al. (1993) estimated that the horizontal hydraulic conductivity ranges from less than 7×10^{-5} or 20 ft/day (Gonzales 1 and Zamora 1) to approximately 4×10^{-4} m/s or 100 ft/day (Charles 5). Horizontal hydraulic conductivity estimates for the Coronado 2 and PSMW 19 wells are not tabulated in Thorn et al. (1993), but they probably lie somewhere between the high and low values given above.

The five-fold range in average horizontal hydraulic conductivity observed among the wells analyzed in this paper can be understood in terms of the Hawley (in press a,b; also see Hawley and Haase, 1992) lithofacies found in the wells. The Gonzales 1 well penetrates nearly equal net thicknesses of lithofacies Ib braided river gravels and lithofacies III basin-floor alluvial/playa/eolian deposits (see Hawley, in press b, Appendix F, for lithologic logs). The lithofacies Ib gravels, in particular, are pumice rich. The Zamora 1 penetrates alternating intervals of lithofacies Ib braided river gravels, lithofacies II basin-floor fluvial/eolian deposits, lithofacies IX basin-floor playa/alluvial flat deposits, and lithofacies III basin-floor alluvial/playa/eolian deposits. The upper portion of the Charles 5 well, in contrast, penetrates lithofacies Ib braided river gravels intermixed with only minor amounts of lithofacies III basin-floor alluvial/playa/eolian deposits and lies within an elongated zone of high-conductivity axial river gravels deposited by the ancestral Rio Grande (Thorn et al., 1993).

Components and magnitudes of specific storage

Specific storage is the volume of water released from storage per volume of aquifer per unit of drawdown and has units of reciprocal length (m^{-1} in this study). Studies of the mechanical response of aquifer systems to pumping have shown that specific storage consists of four parts: (1) a recoverable component associated with the elastic deformation of the aquifer system skeleton, (2) a recoverable component associated with the elastic expansion of water as it is brought from depth to the ground surface, (3) a recoverable component associated with the elastic deformation of the skeletal grains, and (4) a non-recoverable or virgin component associated with inelastic deformation of the aquifer system (Poland, 1984; Van der Kamp and Gale, 1987). Virgin specific storage is typically one to two orders of magnitude greater than the sum of the elastic specific storage components. In the case of an overconsolidated aquifer system, inelastic deformation does not become significant until the preconsolidation stress has been exceeded (Holzer, 1981).

Studies in basin-fill aquifer systems in Arizona and California have produced specific storage estimates for similar systems in the southwestern and western United States. Poland (1984) estimated specific storage components of 6.3×10^{-6} m^{-1} from elastic deformation of the aquifer skeleton, 1.9×10^{-6} m^{-1} from elastic expansion of water, and 6.7×10^{-4} m^{-1} from inelastic deformation of San Joaquin Valley basin-fill sediments near Pixley, California. In this case, the ratio of virgin to elastic specific storage was approximately 80:1. Using data from vertical extensometer sites in the Santa Clara and San Joaquin valleys of California, Helm (1976, 1978) calculated elastic specific storage values ranging from 6.6×10^{-6} m^{-1} to 26.2×10^{-6} m^{-1} and virgin specific storage values ranging from 4.6×10^{-4} m^{-1} to 22.0×10^{-4} m^{-1}, which yield virgin to elastic specific storage ratios of 19:1 to 148:1. Hanson (1989) estimated values of virgin specific storage ranging from 1.5×10^{-5} m^{-1} to 2.0×10^{-4} m^{-1} for basin-fill sediments at vertical extensometer sites in the Tucson Basin and Avra Valley, Arizona. Ratios of virgin to elastic specific storage therefore ranged from 2:1 to 27:1. Epstein (1987) used extensometer-derived elastic specific storage values of 8.0×10^{-6} m^{-1} to 1.0×10^{-5} m^{-1} and virgin specific storage values of 5.0×10^{-4} m^{-1} to 9.0×10^{-4} m^{-1} in computer simulations of land subsidence near Eloy, Arizona, yielding virgin to elastic specific storage ratios of 50:1 to 90:1. Examination of the data tabulated in the studies cited above shows a weak positive correlation between elastic and virgin specific storage values estimated for a given location.

Specific storage data for basin-fill sediments along the Rio Grande valley are limited. Vertical extensometer data collected during recent pumping tests in Albuquerque suggest that the depth-averaged elastic specific storage in the vicinity of the extensometer site is approximately 7×10^{-6} m^{-1}, and estimates derived from

piezometric earth tide response at the same extensometer site range from approximately 3.7×10^{-6} m^{-1} at a depth of 300 m to 5.6×10^{-6} m^{-1} at a depth of 50 m (C. Heywood, U.S. Geological Survey, written comm. June 1, 1995). Haneberg and Freisen (1995) estimated subsidence near the center of the Mimbres Basin of southern New Mexico to be on the order of 0.5 m, compared to a water-level decrease of approximately 35 m. These values yield a specific compaction estimate on the order of 1×10^{-2} and, assuming that the effective aquifer thickness is close to the typical agricultural well screen length of several tens of meters, an inelastic specific storage value on the order of 10^{-4} m^{-1}. This estimate is of the magnitude expected for virgin, rather than elastic, specific storage, as one might expect for a basin that is characterized by land subsidence and earth fissures (Contaldo and Mueller, 1991). Kernodle (1992) was able to replicate observed land subsidence magnitudes in the El Paso, Texas area using an elastic specific storage value of 2.0×10^{-5} m^{-1} in a computer model; however, this simulated value is an order of magnitude greater than elastic specific storage values measured in many other basin-fill aquifer systems and is therefore suspect.

Spatial variability of porosity in the Charles 5 well

Porosity curves for the selected Albuquerque Basin water wells are typically characterized by a 5 to 10% decrease in porosity with depth within the upper several hundred meters, which can be illustrated in different ways. Hawley and Haase (1992), for example, used visual examination of bulk density, sonic travel time, and various porosity geophysical logs as the basis of their conclusion that the systematic top-to-bottom decrease is a result of sediment compaction. Visual recognition of large-scale systematic changes or trends can be complicated, however, by the effects of small-scale stratigraphic variability. Small-scale variations may occur on the scale of meters, decimeters, or centimeters; moreover, the magnitudes of small-scale variations may be as large as or even greater than the magnitude of change associated with the larger-scale trend upon which they are superimposed.

Data from the upper portion (110–549 m) of the Charles 5 well were used in the initial phase of this study to examine the nature of porosity variability in the upper Santa Fe Group aquifer system. The Charles 5 was a deep test hole with a total depth of 984 m (3,230 ft), so only the upper portion of the well penetrating typical upper Santa Fe Group aquifer strata was analyzed in this part of the study. Log data were collected at 0.15-m (6-inch) intervals, and only data from beneath the water table were used in the initial portion of the study.

The depths and combinations in which various lithofacies were found in the upper portion of the Charles 5 well, obtained from Hawley (in press b, Appendix F), are listed in Table 1. Characteristics of the individual lithofacies and sublithofacies are described below.

Lithofacies Ib—River-valley and basin-floor braided stream deposits. Sand and pebble gravel with lenses of silt and clay.

Lithofacies II—Basin-floor fluvial and, locally, eolian deposits. Sand with lenses of pebbly sand, silt, and silty clay.

Lithofacies III—Basin-floor alluvium and playa deposits with local eolian deposits. Interbedded sand, silt, and silty clay, with lenses of pebbly sand.

Lithofacies Vd—Distal to medial piedmont-slope alluvial-fan deposits associated with large watersheds; alluvial-fan distributary channels. Sand and gravel, with lenses of gravelly to nongravelly sand, silt, and clay.

Lithofacies Vf—Distal to medial piedmont-slope alluvial-fan deposits associated with small watersheds; alluvial-fan distributary-channel and debris-flow deposits. Gravelly sand, silt, and clay, with lenses of sand, gravel, and silty clay.

Lithofacies VII—Distal to medial piedmont-slope alluvial-fan distributary-channel and debris-flow deposits. Indurated equivalent of Vd, Vf, and undifferentiated V.

Basic statistics

A porosity cross-plot consisting of 2,870 points shows that, although there is a general correlation between porosity values measured using the two different methods, density porosity tends to be slightly less than neutron porosity (Fig. 2). There are also a number of points, from the top of the sampled interval, for which density porosity is greater than neutron porosity. Nonetheless, the cloud of points does plot sufficiently close to the 1:1 line to conclude that density porosity alone should be an adequate representative of the true porosity value for the aquifer system described in this paper. There is also some correlation between the 11-point variance and the 11-point mean of the porosity, with the highest means and variances obtained for the uppermost portion of the well penetrating lithofacies Ib (Fig. 3).

Cumulative porosity distributions were calculated both for the entire upper portion of the Charles 5 well (110–549 m) as well as for each ocurrence of lithofacies encountered in the upper portion and are summarized in a box plot (Fig. 4). The two uppermost intervals, consisting of lithofacies Ib braided river gravels and mixed lithofacies Ib/III braided river gravels and basin-floor alluvial/playa/eolian deposits, have higher sample means and variances than do deeper intervals. Also, the shallower occurrence of lithofacies Ib has a significantly larger mean and variance than the deeper occurrence of lithofacies Ib. Cumulative distribution plots show that there can also be more difference between the porosity distributions from

TABLE 1—Lithofacies found in the upper portion of the Charles 5 well.

Depth (ft)	Depth (m)	Lithofacies
0–98	0–30	Vf
98–540	30–165	Ib
540–700	165–213	Ib, III
700–870	213–265	Ib
870–1040	265–317	III, Ib
1040–1100	317–335	III
1100–1260	335–384	II, Vd
1260–1560	384–476	Vf, VII
1560–2020	476–616	III, V, VII

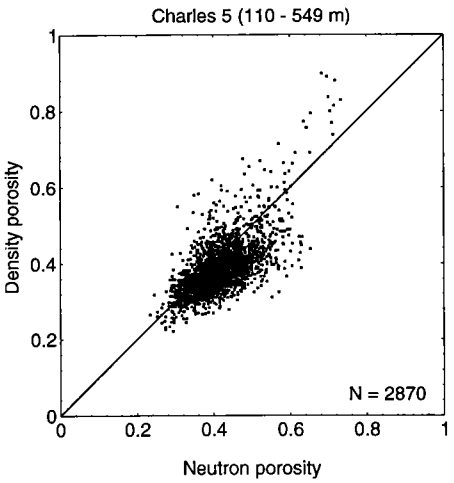

FIGURE 2—Neutron-density porosity cross-plot for the upper portion of the Charles 5 well.

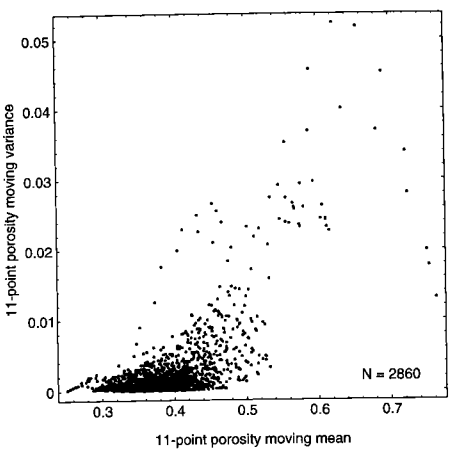

FIGURE 3—Plot of moving sample variance versus moving sample mean for the upper portion of the Charles 5 well.

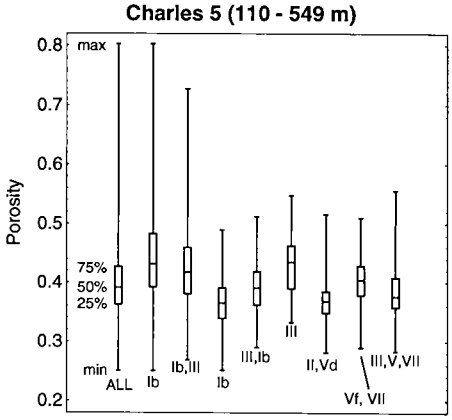

FIGURE 4—Geophysical log porosity quartiles by lithofacies, upper portion of the Charles 5 well.

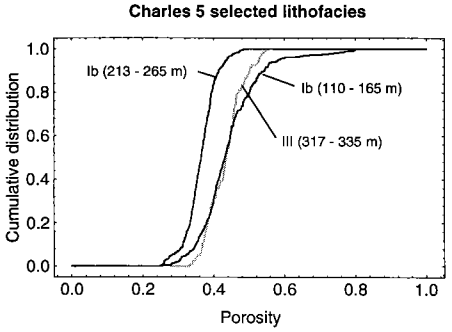

FIGURE 5—Cumulative porosity distributions for the two unmixed occurrences of lithofacies Ib and the single unmixed occurrence of lithofacies III from the upper portion of the Charles 5 well.

two occurrences of the same lithofacies than between occurences of different lithofacies (Fig. 5) The same pattern occurs between the shallow and deep occurrences of mixed lithofacies Ib/III.

The variogram statistic

Scales of spatial variability can be investigated by calculating experimental or empirical variograms, which reflect the difference in magnitude between all possible pairs of spatially correlated random variables separated by a specified distance or lag. The variogram statistic is (Isaaks and Srivastava, 1989)

$$\gamma(h) = \frac{1}{2N_h} \sum_{(i,j)|h_{i,j}=h} (y_i - y_i)^2 \qquad (1)$$

wherein $\gamma = \gamma(h)$ is the variogram statistic, h is the absolute value of the spatial separation or lag between each pair of data points, y is the spatially correlated random variable (i.e., porosity in this study), and N_h is the number of data pairs separated by a lag of h. In contrast to statistics such as the sample mean and sample variance, which require relatively few data, variograms typically require several hundred data points. Features of an idealized variogram include the *sill*, the *range*, and the *nugget*. The sill is a plateau attained at some distance beyond which the variogram statistic is constant and is equal in magnitude to the sample variance. The range is the lag distance at which the sill is reached. A nugget is said to exist when the variogram has a non-zero value at a lag of $h = 0$, typically because there is spatial variability at a scale smaller than the lag increment used to construct the variogram from empirical data. Finally, a *hole effect* is said to exist if the variogram statistic fluctuates about the sill at large lag distances.

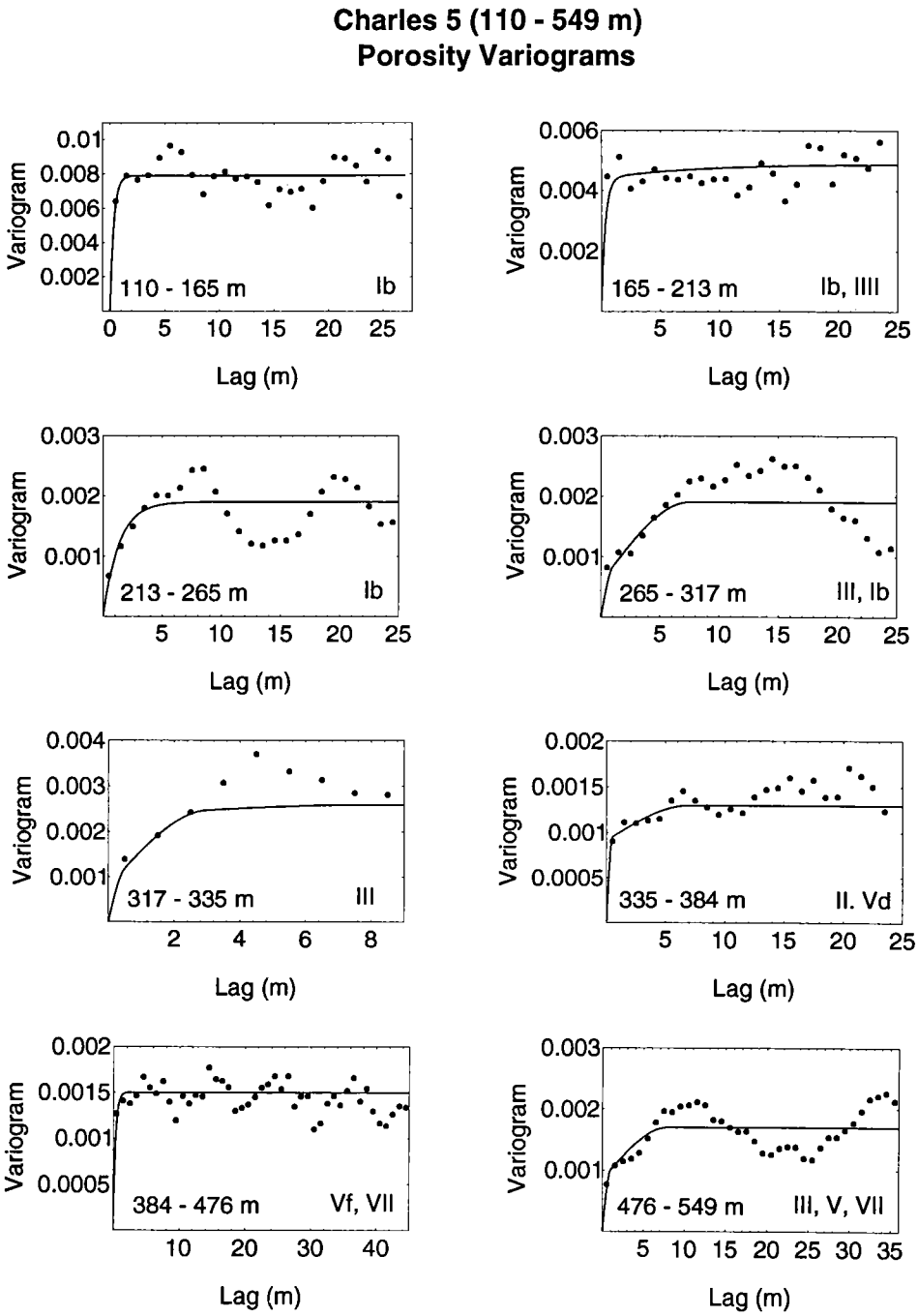

FIGURE 6—Empirical and fitted porosity variograms for the depth intervals listed in Table 1 and statistically summarized in Table 2. Equations for the fitted variograms are given in Table 3.

The forms of real variograms, which can exhibit elaborate spatial correlation structures, commonly depart from the idealized example described above.

Empirical variograms were prepared in order to examine the spatial variability of porosity within each of the eight lithofacies intervals identified by Hawley (in press b, Appendix F) as well as in the undifferentiated upper portion of the well (Figs. 6, 7). Variogram lag intervals were 1.0 ±0.5 m for the lithofacies intervals and 5.0 ±2.5 m for the undifferentiated upper portion. The maximum lag distance calculated for each variogram was one-half the

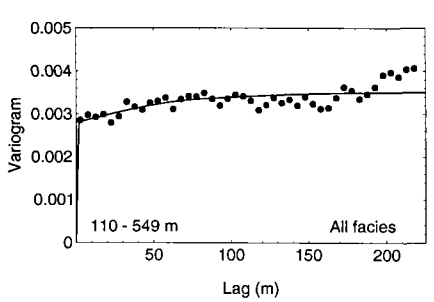

FIGURE 7—Empirical and fitted variograms for undifferentiated porosity data from the upper portion of the Charles 5 well. The fitted variogram equation is given in Table 3.

TABLE 2—Summary of fitted porosity variogram types and ranges, upper portion of Charles 5 well.

Lithofacies	Depth (m)	Variogram type	Variogram range(s) (m)
ALL	110–549	Nested spherical	2, 80, 200
Ib	110–165	Exponential	1
Ib, III	165–213	Nested exponential	1, 25
Ib	213–265	Exponential	4
III, Ib	265–317	Nested spherical	1, 7, 5
III	317–335	Nested spherical	0.5, 3, 8
II, Vd	335–384	Nested spherical	0.5, 7
Vf, VII	384–476	Exponential	1
III, V, VII	476–549	Nested spherical	1, 8

interval thickness, beyond which the number of data pairs and the quality of the variogram decreased sharply. Most of the empirical variograms show small ranges, typically on the order of a meter or so, as well as distinct hole effects that indicate cyclicity in the data. Nugget effects occurred for lithofacies Ib (110–165 m), Ib/III (165–213 m), Vf/VII (384–476 m), and the undifferentiated data set (110–549 m), implying the existence of correlation scales shorter than the minimum lag values of 1.0 and 5.0 m. Porosity variograms for lithofacies Ib/II (165–213 m), III (317–335 m), and II/Vd (335–384 m) do not reach a sill and may reflect underlying nonstationarity in the data set.

Model variograms were fitted to the empirical variograms by trial-and-error, beginning with a single exponential variogram of the form (Isaaks and Srivastava, 1989)

$$\gamma(h) = \sigma^2 \left[1 - \exp\left(-\frac{3h}{r} \right) \right] \quad (2)$$

or a single spherical variogram of the form

$$\gamma(h) = \sigma^2 \left[\frac{3h}{2r} - \frac{1}{2} \left(\frac{h}{r} \right)^3 \right] \quad (3)$$

where σ is the sample variance, h is the lag distance, and r is the variogram range. No nuggets were allowed in the model variograms. If an empirical variogram could not be readily modeled using either of the two variograms shown above, a nested variogram was used beginning with two and, if necessary, proceeding to three levels of spatial correlation. In order to reduce the complexity of fitting nested variograms, it was arbitrarily decided that all components would be of the same type (e.g., two exponential variograms could be nested, but not one exponential and one spherical). Each nested variogram component was weighted such that the weights summed to unity in order to insure that the sill would remain equal to the sample variance.

Fitted variogram types and ranges are summarized in Table 2, fitted variogram equations are given in Table 3, and the fitted variograms are plotted as solid lines in Figs. 6 and 7. Six of the eight lithofacies variograms required nested models, with ranges from 0.5 to 25 m, whereas the undifferentiated variogram required a nested model with ranges of 2, 80, and 200 m. Thus, porosity in sediments penetrated by the upper portion of the Charles 5 varies at the bedding scale, the lithofacies scale, and the formation scale.

Depth-porosity curves and virgin specific storage

After the initial evaluation of porosity variability in the Charles 5 well was completed, depth-porosity curves for the Charles 5, Coronado 2, Gonzales 1, PSMW 19, and Zamora 1 wells were estimated by fitting model exponential and logarithmic type curves to the porosity data sets. Density-porosity values were selected for the depth-porosity-curve analysis because they are common to virtually all Albuquerque Basin water-well-log suites, and porosity can be easily calculated if bulk density rather than density porosity is given on the log. Neutron-porosity values, in contrast, are sometimes given in API units that cannot be converted directly to porosity. Sonic logs, from which porosity can also be calculated, are rare except for recent wells. As illustrated in a previous section, there does not appear to be a significant difference between neutron and density porosity values for the upper portion of the Charles 5 well, and it is assumed that the same holds true for other Albuquerque Basin water wells. One would ideally like to corroborate geophysical log porosity estimates with core data; however, none were available for this project.

Model compaction curves

The two depth-porosity-curve models used were a negative exponential function of the form (Athy, 1930)

$$n = n_0 \exp(-z/z_0) \quad (4)$$

and a logarithmic function of the form (Dickinson, 1953; Helm, 1984)

$$n = n_0 + c \ln(z/z_0). \quad (5)$$

In equations (4) and (5), n is porosity, z is depth, and n_0, c, and z_0 are empirical constants. Note, however, that n_0 and z_0 will have different values for each of the two depth-porosity-curve models, so that a value estimated by fitting one of the models to a data set cannot be inserted into the other model. In this paper, the terms "exponential type" and "logarithmic type", respectively, are used in reference to the depth-porosity curves described by equations (4) and (5).

Athy (1930) originally suggested values of $n_0 = 0.48$ and $z_0 = 714$ m for equation (4) based on his investigation of shales in Oklahoma (depth converted from feet to meters). Although Dickinson (1953) plotted porosity vs. depth for Gulf Coast shales and drew through his empirical data points a logarithmic curve, he did not write out equation (5) or otherwise explicitly discuss the logarithmic form of the curve. Helm (1984), who was the first to explicitly write out equation (5) and suggest that it was a model depth-porosity curve fundamentally different from that of Athy (1930), calculated values of $n_0 = 0.05$, $c = -0.103$, and $z_0 = 10{,}000$ m for Dickinson's curve.

Model depth-porosity curve parameters were estimated using the Levenberg–Marquardt algorithm for nonlinear curve fitting as implemented in the computer program *Mathematica* (Boyland et al., 1992; also see Press et al., 1992, pp. 678–683 for a detailed description of the algorithm). The empirical constants were constrained during the regressions so that $0 \le n_0 \le 1$, $500 \le z_0 \le 1{,}500$ m, and $-1 \le c \le 0$. Data sets were read directly from ASCII files supplied by the geophysical logging contractors, and spurious values near the top of the log were edited out by hand. Because density porosity values do not appear to change substantially between the saturated zone and the vadose zone, porosity values above and below the static water level were used for depth-porosity curve fitting.

TABLE 3—Summary statistics and modeled porosity variograms for the upper portion of the Charles 5 well.

Lithofacies (depth)	n	Mean	Variance	Modeled Variogram
All (110–549 m)	2870	0.40	0.0035	$\gamma(h) = 0.0035\left\{0.8\left[\frac{3}{2}\left(\frac{h}{2}\right)-\frac{1}{2}\left(\frac{h}{2}\right)^3\right]+0.1\left[\frac{3}{2}\left(\frac{h}{80}\right)-\frac{1}{2}\left(\frac{h}{80}\right)^3\right]+0.1\left[\frac{3}{2}\left(\frac{h}{200}\right)-\left(\frac{h}{200}\right)^3\right]\right\}$
Ib (110–165 m)	358	0.44	0.0079	$\gamma(h) = 0.0079\left[1-\exp\left(-\frac{3h}{1}\right)\right]$
Ib/III (165–213 m)	320	0.42	0.0049	$\gamma(h) = 0.0049\left\{0.9\left[1-\exp\left(-\frac{3h}{1}\right)\right]+0.1\left[1-\exp\left(-\frac{3h}{25}\right)\right]\right\}$
Ib (213–265 m)	340	0.36	0.0019	$\gamma(h) = 0.0019\left[1-\exp\left(-\frac{3h}{4}\right)\right]$
III/Ib (265–317 m)	340	0.39	0.0019	$\gamma(h) = 0.0019\left\{0.3\left[\frac{3}{2}\left(\frac{h}{1}\right)-\frac{1}{2}\left(\frac{h}{1}\right)^3\right]+0.7\left[\frac{3}{2}\left(\frac{h}{7.5}\right)-\frac{1}{2}\left(\frac{h}{7.5}\right)^3\right]\right\}$
III (317–335 m)	120	0.43	0.0026	$\gamma(h) = 0.0026\left\{0.3\left[\frac{3}{2}\left(\frac{h}{0.5}\right)-\frac{1}{2}\left(\frac{h}{0.5}\right)^3\right]+0.6\left[\frac{3}{2}\left(\frac{h}{3}\right)-\frac{1}{2}\left(\frac{h}{3}\right)^3\right]+0.1\left[\frac{3}{2}\left(\frac{h}{8}\right)-\frac{1}{2}\left(\frac{h}{8}\right)^3\right]\right\}$
II/Vd (335–384 m)	317	0.37	0.0013	$\gamma(h) = 0.0013\left\{0.7\left[\frac{3}{2}\left(\frac{h}{0.5}\right)-\frac{1}{2}\left(\frac{h}{0.5}\right)^3\right]+0.3\left[\frac{3}{2}\left(\frac{h}{7}\right)-\frac{1}{2}\left(\frac{h}{7}\right)^3\right]\right\}$
Vf/VII (384–476 m)	597	0.40	0.0015	$\gamma(h) = 0.0015\left[1-\exp\left(-\frac{3h}{1}\right)\right]$
III/V/VII (476–549 m)	478	0.38	0.0017	$\gamma(h) = 0.0017\left\{0.5\left[\frac{3}{2}\left(\frac{h}{1}\right)-\frac{1}{2}\left(\frac{h}{1}\right)^3\right]+0.5\left[\frac{3}{2}\left(\frac{h}{8}\right)-\frac{1}{2}\left(\frac{h}{8}\right)^3\right]\right\}$

Calculation of virgin specific storage

Assuming that the compressibility of water is negligible, that all deformation occurs as vertical compaction, and that all sediments are normally consolidated, virgin specific storage is related to porosity and the porosity gradient by (Helm, 1984)

$$S'_{skv} = -\frac{1}{(1-n)^2(G-1)}\frac{dn}{dz} \qquad (6)$$

in which n is porosity, G is the specific gravity of the solids composing the basin fill, and z is depth. This model implicitly assumes that the compacting sediments were originally homogeneous, with no large-scale changes in initial porosity or compressibility with depth. The average virgin specific storage between depths z_1 and z_2 can be found by integrating equation (6) as follows:

$$\overline{S}'_{skv} = \frac{1}{z_2-z_1}\int_{z_1}^{z_2} S'_{skv}\,dz \qquad (7)$$

The dimensionless ratio of vertical aquifer compaction to head decrease, which is sometimes referred to as specific compaction, is given by (Helm, 1984)

$$\frac{\Delta b}{\Delta h} = (z_2-z_1)\,\overline{S}'_{skv} = \int_{z_1}^{z_2} S'_{skv}\,dz \qquad (8)$$

where Δb is the decrease in aquifer thickness and Δh is the decrease in hydraulic head. Thus, the calculation of virgin specific storage and specific compaction is simple once a depth-porosity curve is obtained for a given well.

Results

Fitted depth-porosity curves are superimposed on porosity logs for the five wells in Figs. 8 through 12, and the best-fit depth-porosity curve parameters are listed in Table 4. Average virgin specific storage for all but one of the wells was on the order of 10^{-4} m^{-1}, and specific compaction ranged between 0.02 and 0.10. These values were averaged over the depth interval of 200 to 400 m with the exception of the PSMW 19 results, which were averaged over the depth interval of 100 to 300 m because the well is only about 270 m deep. Most of the difference between the exponential and logarithmic curves occurs at very shallow depths, so the virgin specific storage and specific compaction estimates calculated using the two curves were similar. With the exception of the Gonzales 1 well, which is discussed below, goodness-of-fit (r^2) values ranged between 0.10 and 0.49, suggesting that the fitted depth-porosity curves can account for about 10 to 50% of the observed porosity variability. These values are consistent with the weights assigned to the nested porosity variogram components for the undifferentiated upper portion of the Charles 5 well, in which the 80 and 200 m range components each accounted for 10% of the sill.

The only well for which problems were encountered was the Gonzales 1, for which porosity values were unusually high (in some cases approaching 1.0) above a depth of 125 m. The reason for these unusually high values is unclear, and the geophysical log for the nearby Gonzales 2 well gave no indication of similarly high values. Therefore, depth-porosity curve fitting was performed using only porosity data collected between 125- and 550-m depth. Although the fitted exponential curve yielded reasonable but somewhat low values, the fitted logarithmic curve is very steep and yielded virgin specific storage and specific compaction values an order of magnitude smaller than the other wells. The fitted depth-porosity curves for the Gonzales 1 were most likely affected by some combination of the

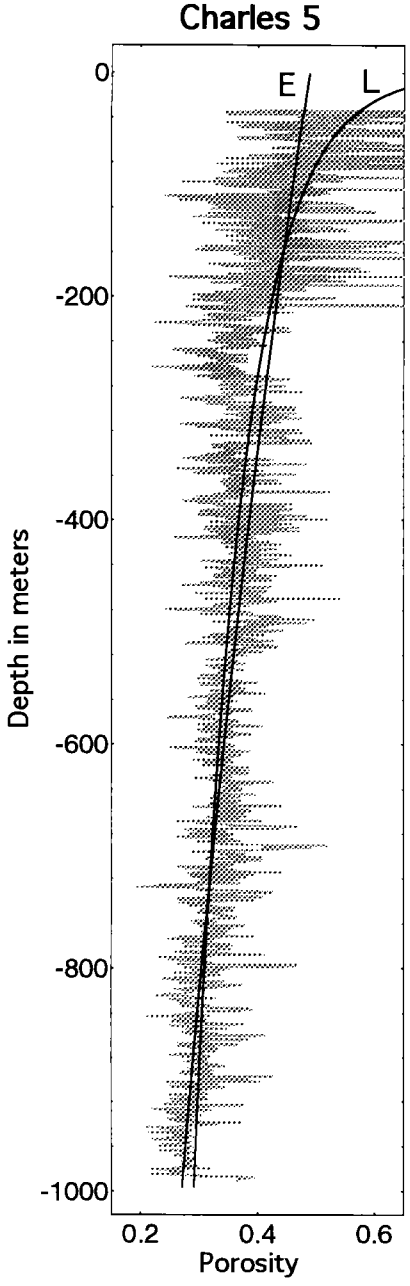

FIGURE 8—Best-fit exponential type and logarithmic type depth-porosity curves superimposed on the density porosity log for the Charles 5 well. **E**, exponential curve; **L**, logarithmic curve. Depth-porosity curve parameters are in Table 4.

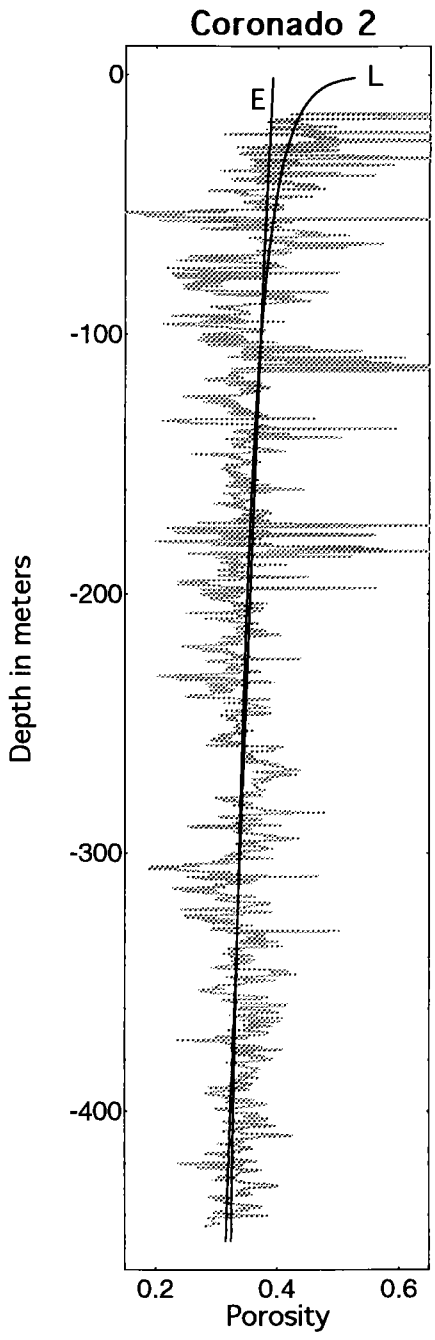

FIGURE 9—Best-fit exponential type and logarithmic type depth-porosity curves superimposed on the density-porosity log for the Coronado 2 well. **E**, exponential curve; **L**, logarithmic curve. Depth-porosity curve parameters are in Table 4.

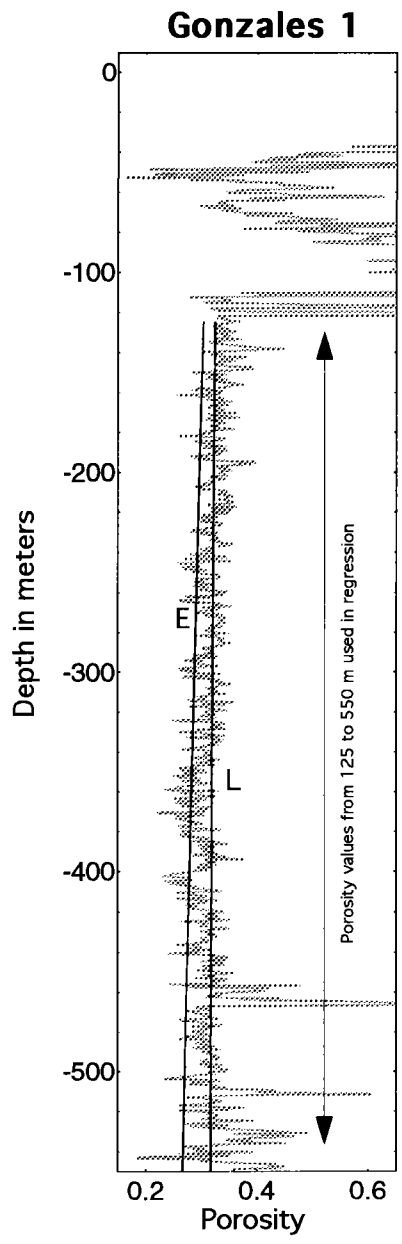

FIGURE 10—Best-fit exponential type and logarithmic type depth-porosity curves superimposed on the density-porosity log for the Gonzales 1 well. **E**, exponential curve; **L**, logarithmic curve. Depth-porosity curve parameters are in Table 4.

absence of high porosity values at shallow depths and a systematic increase in porosity values at depths greater than 400 m.

Discussion

Analysis of variograms constructed using porosity data from the Charles 5 geophysical logs shows that the porosity of the basin-fill sediments is spatially correlated in the vertical direction over scales ranging from decimeters to hundreds of meters. Nested or multicomponent variograms were required to model the spatial correlation structure of porosity for six of the eight lithofacies intervals examined in this study, as well as for undifferentiated sediments penetrated by the upper portion of the Charles 5 well. Nested correlation structures imply that porosity in the upper Santa Fe Group is spatially correlated on several different scales (e.g., Gelhar, 1993). Small- to medium-scale variations in porosity, say those that occur over distances on the order of 0.5 to 10 meters, reflect differences in porosity among individual beds or architectural elements (Phillips and Wilson, 1989; Davis et al., 1993; Macfarlane et al., 1994). Large-scale variations, in this case those that occur over ranges of hundreds of meters (or perhaps more), are inferred to be an effect of sediment compaction rather than large-scale stratigraphic changes; however, these changes may be difficult to discern because they contribute less to the total variability of porosity than do the small-scale variations. For example, the modeled porosity variogram for the undifferentiat-

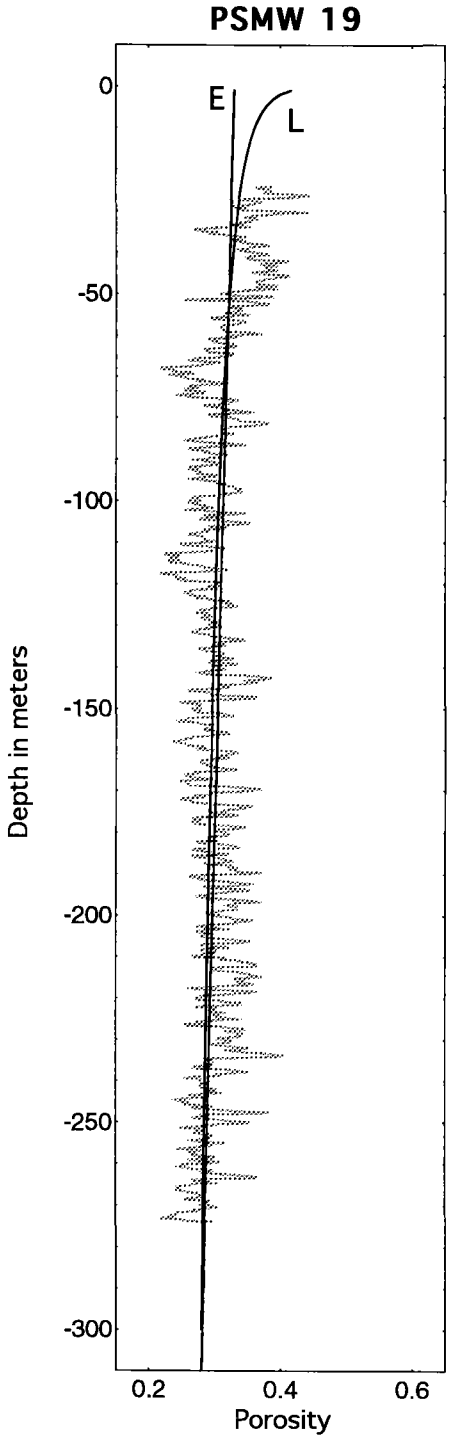

FIGURE 11—Best-fit exponential type and logarithmic type depth-porosity curves superimposed on the density-porosity log for the PSMW 19 well. **E**, exponential curve; **L**, logarithmic curve. Depth-porosity curve parameters are in Table 4.

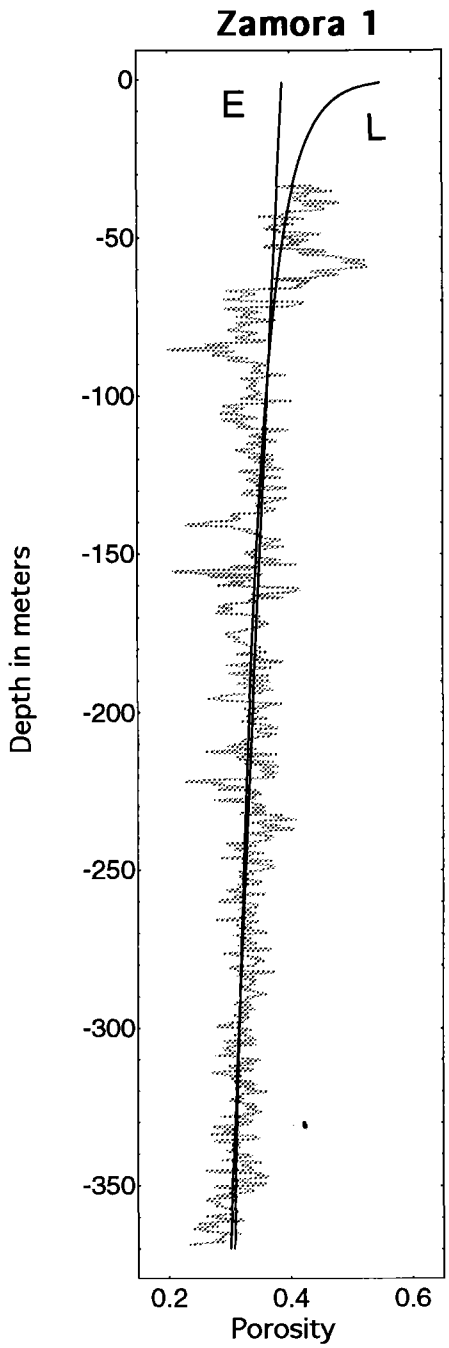

FIGURE 12—Best-fit exponential type and logarithmic type depth-porosity curves superimposed on the density-porosity log for the Zamora 1 well. **E**, exponential curve; **L**, logarithmic curve. Depth-porosity curve parameters are in Table 4.

ed Charles 5 data set is weighted in such a manner that the 2-m component contributes 80% of the variability whereas the 80- and 200-m components each contribute 10% of the variability.

The inference of compaction-induced porosity variability is supported by three lines of evidence. First, similar systematic changes in porosity have been attributed to sediment compaction in many other basins (Athy, 1930; Dickinson, 1953; Baldwin and Butler, 1985), and it is unlikely that large-scale stratigraphic variability in the Albuquerque Basin coincidentally follows the same pattern as compaction effects in other basins. Second, there is a correlation between porosity means and variances calculated on a lithofacies-by-lithofacies basis from the Charles 5 data, and both the means and variances decrease with depth. One might expect more highly compacted (i.e., more deeply buried) sediments to have smaller porosity means and variances than less highly compacted (i.e., less deeply buried) sediments. Third, lithofacies penetrated at shallow depths are more porous than occurrences of the same lithofacies penetrated at greater depths. In the Charles 5 well, for example, the shallow occurrence of lithofacies Ib is more porous than the deeper occurrence of lithofacies Ib.

Nonlinear fitting of exponential and logarithmic type depth-porosity curves to porosity data sets from four wells in and around Albuquerque yielded virgin specific storage estimates on the order of 10^{-4} m^{-1} for depths of 200 to 400 m. These values are the same magnitude as estimates obtained by others for other basin-fill aquifer systems in the western United States (e.g., Poland, 1984; Epstein, 1987; Hanson, 1989). The geophysical logs for a fifth well, the Gonzales 1, contain unrealistically high porosity data for shallow depths and yield unusually small, and therefore unreliable, values. This illustrates the importance of collecting shallow porosity data in order to constrain depth-porosity curve parameters. Specific compaction estimates for the same four wells ranged from 0.02 to 0.10, implying that long-term aquifer compaction may amount to as much as 10% of the water-level decrease. The goodness-of-fit values obtained for the depth-porosity curves suggest that compaction effects can account for 10% to 50% of the total porosity variability, which is in fair agreement with the value of 20% suggested by the nested variogram weights.

One of the most interesting results of this study is the finding that the Charles 5 well, which had the largest virgin specific storage estimate (that is to say, the greatest compaction potential), also has the highest average horizontal hydraulic conductivity. Unlike the other wells studied, the Charles 5 well penetrates primarily lithofacies Ib river gravels, which one would not expect to be particularly compactible. One possible explanation is that the sample of four wells with reliable depth-porosity curves is simply too small, and the calculation of the highest virgin specific storage value for the Charles 5 well is a statistical fluke. Another possible explanation is that lithofacies Ib river gravels, which are pumice rich, are truly more compactible than the sediments penetrated by the other wells examined in this paper. Further analysis will be needed to discern between the two possibilities.

With the exception of isolated occurrences of subsidence and structural damage in the North Valley area, which are believed to have resulted from dewatering of the shallow alluvial aquifer and associated wetlands rather than the upper Santa

TABLE 4—Best-fit compaction curve parameters and virgin specific storage estimates for selected Albuquerque Basin water wells. The Generic curve was calculated using model curve parameters proposed by Athy (1930) for the exponential type curve and by Helm (1984) for the logarithmic type curve.

	Exponential type curve $n = n_0 \exp(-z/z_0)$					Logarithmic type curve $n = n_0 + c\ln(z/z_0)$					
	n_0	z_0 (m)	r^2	$\overline{S}'_{skv}$ (m^{-1})	$\Delta b/\Delta h$	n_0	c	z_0 (m)	r^2	$\overline{S}'_{skv}$ (m^{-1})	$\Delta b/\Delta h$
Generic	0.48	714		8.1×10^{-4}	0.16	0.05	-0.103	10,000		7.1×10^{-4}	0.14
Charles 5	0.49	1690	0.41	4.2×10^{-4}	0.08	0.30	-0.084	851	0.49	4.8×10^{-4}	0.10
Coronado 2	0.39	2094	0.093	2.2×10^{-4}	0.04	0.31	-0.032	752	0.13	1.6×10^{-4}	0.03
Gonzales 1	0.32	3222	0.85	1.1×10^{-4}	0.02	0.32	-0.0057	492	0.053	2.6×10^{-5}	0.005
PSMW 19	0.33	1875	0.10	2.0×10^{-4}	0.04	0.28	-0.024	365	0.17	2.4×10^{-4}	0.05
Zamora 1	0.39	1451	0.27	2.8×10^{-4}	0.06	0.29	-0.041	635	0.32	1.8×10^{-4}	0.04

Fe Group aquifer system (Kernodle, 1995), there is no convincing evidence of widespread land subsidence in the Albuquerque area despite heavy pumping and water-level decreases that locally exceed 50 m (see Thorn et al., 1993 for water-level-decline maps). In contrast, water-level decreases of 35 m and less have produced widespread land subsidence and earth fissures in the Mimbres Basin south of Deming, New Mexico (Contaldo and Mueller, 1991; Haneberg and Friesen, 1995). The most likely explanation for the lack of subsidence in and around Albuquerque is that the upper Santa Fe Group aquifer system is overconsolidated, meaning that in the past the aquifer system has been subjected to greater lithostatic stress than it is being subjected to today. Holzer (1981) has shown that if an aquifer system has been overconsolidated, land subsidence is minimal until the reduction in effective confining stress brought about by ground-water overdraft exceeds the preconsolidation stress, which is the maximum effective stress to which the system has been subjected in the past. Because the ground water exerts an up-ward-directed buoyant force on the aquifer skeleton, a reduction in water level (and therefore pore-water pressure) is mechanically equivalent to an increase in the weight of the overlying sediments.

Once the preconsolidation stress is exceeded, according to the data collected by Holzer (1981), land subsidence occurs rapidly.

The postulated overconsolidation of the upper Santa Fe Group aquifer system is probably a result of the Pleistocene incision of the Rio Grande valley, which produced geomorphic features such as the Llano de Albuquerque—a relic of the pre-incision basin floor—and stream terraces well above the current river level. The difference in elevation between the Llano de Albuquerque and the modern river level suggests that as much as 100 m of sediment may have been removed from the center of the basin. Assuming that the pre-incision water table had the same relationship with the ground surface as did the Holocene pre-development water table, the difference between the preconsolidation stress and the current effective lithostatic stress for the upper Santa Fe Group aquifer system should be equal to the buoyant unit weight of the basin fill multiplied by the depth of incision or, equivalently, the change in water-table elevation. Because the saturated unit weight of unconsolidated siliciclastic sediments is about twice the unit weight of water, the stress difference is approximately equal to the pressure at the base of a column of water equal in height to the inferred depth of incision (i.e., on the order of 100 ±20 m H_2O or 1000 ±200 kPa). The low values are obtained by using a saturated bulk density of 1,800 kg/m^3, the average values are obtained by using a saturated bulk density of 2000 kg/m^3, and the high values are obtained by using a saturated bulk density of 2,200 kg/m^3. Therefore, it appears that there is little potential for widespread subsidence in the immediate future. Over the long term, however, there is a considerable potential for widespread land subsidence if drawdown approaches the 80–120-m range. It must be emphasized, however, that the preconsolidation stress estimates given above are based on subjective geomorphic criteria and are therefore imprecise and highly speculative. More accurate estimates of the preconsolidation stress, which are necessary to adequately assess the subsidence potential, can be obtained either by laboratory testing of samples or by continuing to withdraw ground water and noting the amount of drawdown that is necessary to induce widespread land subsidence in the Albuquerque area.

ACKNOWLEDGMENTS—The work described in this paper was conducted under a cooperative agreement between the City of Albuquerque and the New Mexico Bureau of Mines and Mineral Resources. John Hawley developed the lithofacies classification system referred to in this paper and contributed many hours of insight on the hydrogeologic setting of the Albuquerque Basin. We would all be much poorer without John's enthusiasm and vision. Charles Heywood (U.S. Geological Survey) provided Albuquerque and El Paso extensometer data for comparison with the estimates presented in this paper. Reviews by Michael Campana, Donald Helm, and Charles Heywood helped to improve the quality of this paper and are greatly appreciated.

References

Athy, L. F., 1930, Density, porosity, and the compaction of sediments: American American Association of Petroleum Geologists, Bulletin, v. 14, pp. 1–24.

Baldwin, B., and Butler, C. O., 1985, Compaction curves: American Association of Petroleum Geologists, Bulletin, v. 69, pp. 622–626.

Boyland, P., Keiper, J., Martin, E., Novak, J., Petkovsek, M., Skiena, S., Vardi, I., Wenzlow, A., Wickham-Jones, T., Withoff, D., 1992, Guide to standard Mathematica packages (2nd ed.): Champaign, Illinois, Wolfram Research, Inc., 384 pp.

Contaldo, G. J., and Mueller, J. E., 1991, Earth fissures of the Mimbres Basin, southwestern New Mexico: New Mexico Geology, v. 13, pp. 69–74.

Davis, J. M., Lohman, R. C., Phillips, F. M., Wilson, J. L., and Love, D. W., 1993, Architecture of the Sierra Ladrones Formation, central New Mexico: depositional controls on the permeability correlation structure: Geological Society of America Bulletin, v. 105, pp. 998–1007.

Dickinson, G., 1953, Geological aspects of abnormal reservoir pressures in Gulf Coast Louisiana: American Association of Petroleum Geologists, Bulletin, v. 37, pp. 410–432.

Epstein, C. J., 1987, Hydrologic and geologic factors affecting land subsidence near Eloy, Arizona: U.S. Geological Survey, Water-resources Investigations, Report 87–4143.

Gelhar, L. W., 1993, Stochastic subsurface hydrology: Englewood Cliffs, NJ, Prentice-Hall, 390 pp.

Haneberg, W. C., 1988, Some possible effects of consolidation on growth fault geometry: Tectonophysics, v. 148, pp. 309–316.

Haneberg, W. C. and Friesen, R. L., 1995, Tilts, strains, and ground-water levels near an earth fissure in the Mimbres Basin, New Mexico: Geological Society of America, Bulletin, v. 107, pp. 316–326.

Hanson, R. T., 1989, Aquifer-system compaction, Tucson Basin and Avra Valley, Arizona: U.S. Geological Survey, Water-resources Investigations, Report 88–4172.

Hawley, J. W., in press a, Hydrogeologic setting of the Albuquerque Basin: New Mexico Bureau of Mines and Mineral Resources, Open-file Report 402–B.

Hawley, J. W., in press b, Hydrogeologic framework of basin areas in Bernalillo and southern Sandoval Counties; *in* Haneberg, W. C., and Hawley, J. W. (eds), Characterization of hydrogeologic units in the northern Albuquerque Basin: New Mexico Bureau of Mines and Mineral Resources, Open-file Report 402–C.

Hawley, J. W., and Haase, C. S., 1992, Hydrogeologic framework of the northern Albuquerque Basin: New Mexico Bureau of Mines and Mineral Resources, Open-file Report 387.

Helm, D. C., 1976, Estimating parameters of compacting fine-grained interbeds within a confined aquifer system by a one-dimensional simulation of field observations: International Association of Hydrological Sciences, Publication no. 121, pp. 145–156.

Helm, D. C., 1978, Field verification of a one-dimensional mathematical model for transient compaction and expansion of a confined aquifer system: American Society of Civil Engineers, Proceedings of the Specialty Conference on Verification of Mathematical and Physical Models in Hydraulic Engineering, College Park, Maryland, August 9–11, 1978, pp. 189–196.

Helm, D. C., 1984, Field-based computational techniques for predicting subsidence due to fluid withdrawal; *in* Holzer, T. L. (ed.), Man-induced land subsidence: Geological Society of America, Reviews in Engineering Geology VI, pp. 1–22.

Holzer, T. L., 1981, Preconsolidation stress of aquifer systems in areas of induced land subsidence: Water Resources Research, v. 17, pp. 693–704.

Isaaks, E. H., and Srivastava, R. M., 1989, Applied geostatistics: New York, Oxford University Press, 561 pp.

Kernodle, J. M., 1992, Results of simulations by a preliminary numerical model of land subsidence in the El Paso, Texas, area: U.S. Geological Survey, Water-resources Investigations, Report 92–4037.

Kernodle, J. M., 1995, Simulation of ground-water flow in the Albuquerque Basin, central New Mexico, 1901-1994, with projections to 2020: U.S. Geological Survey, Water-resources Investigations, Report 94–4251, 114 pp.

Macfarlane, P. A., Doveton, J. H., Feldman, H. R., Butler, J. J., Jr., Combes, J. M., and Collins, D. R., 1994, Aquifer/aquitard units of the Dakota aquifer system in Kansas: methods of delineation and sedimentary architecture effects on ground-water flow and flow properties: Journal of Sedimentary Research, v. B64, pp. 464–480.

Phillips, F. M., and Wilson, J. L., 1989, An approach to estimating hydraulic conductivity spatial correlation scales using geological characteristics: Water Resources Research, v. 25, pp. 141–143.

Poland, J. F., 1984, Mechanics of land subsidence due to fluid withdrawal; *in* Poland, J. F., (ed.), Guidebook to studies of land subsidence due to ground-water withdrawal: UNESCO, Studies and Reports in Hydrology 40, pp. 37–54.

Press, W. H., Teukolsky, S. A., Vetterling, W. T., and Flannery, B. P., 1992, Numercial recipes in FORTRAN (2nd ed.): Cambridge, UK, University Press, 963 pp.

Thorn, C. R., McAda, D. P., and Kernodle, J. M., 1993, Geohydrologic framework and hydrologic conditions in the Albuquerque Basin, central New Mexico: U.S. Geological Survey, Water-resources Investigations, Report 93–4149, 106 pp.

Van der Kamp, G., and Gale, J. E., 1983, Theory of earth tide and barometric effects in porous formations with compressible grains: Water Resources Research, v. 19, pp. 538–544. □